Phys. Med. Biol. **54** (2009) 699–713 doi:10.1088/0031-9155/54/3/015

Local complex permittivity measurements of porcine skin tissue in the frequency range from 1 GHz to 15 GHz by evanescent microscopy

Richard A Kleismit[1,2], **Gregory Kozlowski**[1,3], **Brent D Foy**[1], **Barbara E Hull**[4] **and Marian Kazimierczuk**[2]

[1] Department of Physics, Wright State University, 3640 Col. Glenn Hwy, Dayton, OH 45435-0001, USA
[2] Department of Electrical Engineering, Wright State University, 3640 Col. Glenn Hwy, Dayton, OH 45435-0001, USA
[3] Department of Materials Science and Metallurgy, University of Cambridge, Pembroke Str., Cambridge, CB2 3QZ, UK
[4] Department of Biological Sciences, Wright State University, 3640 Col. Glenn Hwy, Dayton, OH 45435-0001, USA

E-mail: richard.kleismit@wright.edu

Received 30 July 2008, in final form 2 December 2008
Published 9 January 2009
Online at stacks.iop.org/PMB/54/699

Abstract

The near-field evanescent microwave microscope is based on a coaxial transmission line resonator with a silver plated tungsten tip protruding through an end-wall aperture. The sensor is used to measure the local dielectric properties of porcine skin in the frequency range from 1 GHz to 15 GHz. The dielectric property of the skin within the near field of the tip frustrates the electric field and measurably changes the transmission line's resonant frequency and quality factor (Q). The shift of the resonator's frequency and Q is measured as a function of tip–sample separation, and a quantitative relationship between the real and imaginary parts of the local dielectric constant using the method of images is established. The associated changes in quality factor image scans of subsurface tissue structure and dielectric properties of skin surface lesions are presented.

(Some figures in this article are in colour only in the electronic version)

1. Introduction

Evanescent microwave techniques of material characterization have been used in a large number of nondestructive testing (NDT) applications some of which could potentially be used for biological studies (Anlage *et al* 2001, Gao and Xiang 1998, 2002, Tabib-Azar *et al* 1999a, Tabib-Azar and LeClair 1999). Several research groups, including our own, have used

evanescent microscopy to characterize impurities and residual stress in semiconductors and superconductors, defects and non-uniformities in composite materials and samples covering the entire conductivity range (metallic to insulating) (Kleismit *et al* 2005a, 2005b, Tabib-Azar *et al* 1999b). In particular, evanescent microwave microscopy can be used to characterize non-uniformities in biological samples and is favorably suited for measuring conductivity, permittivity and density variations. Microwave properties are a function of complex permittivity, permeability, and free carrier concentration. In most biological tissues, moisture content, ionic species such as Na^+ and K^+, free radicals and iron content of blood serum affect the conductivity significantly. These parameters along with density variations, which affect the dielectric constant, can be mapped and quantified through evanescent microwave microscopy. A significant strength of the microwave evanescent field is its ability to penetrate depth-wise into a biological sample and sense localized quantitative material changes *in situ* without this exponentially decaying field altering the sample properties.

Several previous studies of the dielectric properties of skin tissue have been performed using microwave probes (Olawale *et al* 2005, Gabriel *et al* 1996a, 1996b). These studies exhibited dielectric constants between 20 and 85 over a frequency range of 1–20 GHz. Over the same frequency range, the dielectric loss measurements were between 0.1 and 35 with a minimum between 2 GHz and 3 GHz. These previous studies used microwave probes that are open-ended with diameters in the range 1.49–3.5 mm. These open-ended-type probes are mixed mode in the near field, which emit an evanescent field in combination with a propagative wave, but only make use of the propagative component for measurements. In contrast, the probe used in this study is not open-ended and utilizes an end-wall reflective aperture that is sized to cutoff for the measurement frequency, which blocks the propagative wave and emits a purely evanescent field utilized for measurements. This evanescent design will create less athermal stress than the mixed mode probes due to the absence of the propagative wave. In addition, higher spatial resolutions are possible because the probe tip, which extends through the reflective aperture, can be sharpened to a small radius of 10 μm extending through an aperture of 350 μm. This design results in highly localized tissue measurements capable of distinguishing subsurface features.

The objective of this study is to utilize the evanescent microwave probe to investigate the complex permittivity of excised porcine skin tissue samples in the range of frequency from 1 GHz to 15 GHz. This investigation presents the experimental results of probe scan images and the specific local complex dielectric measurements of tissue lesions, surface burns and histological tissue structures utilizing the evanescent microscopy system shown in figure 1. To our knowledge, no previous studies using microwave probe techniques have examined the dielectric properties of porcine skin with lesions or burns, or have attempted to correlate the dielectric properties and conductivity with histological tissue structures such as blood vessels or glandular ducts. A quantitative relationship between the real and imaginary parts of the local dielectric constant and the changes in resonator frequency and Q using the method of images is also presented.

2. Materials and methods

2.1. Measurement system

The resonator probe is based on an open-circuit $\lambda/4$ transmission line and is constructed from an 85-mil., semi-rigid, copper, coaxial transmission line indicated in figure 2. In constructing the probe, the center conductor was removed along with the Teflon insulator. The transmission-line resonator was then reconstructed by casting a sharpened, sterling silver, center conductor

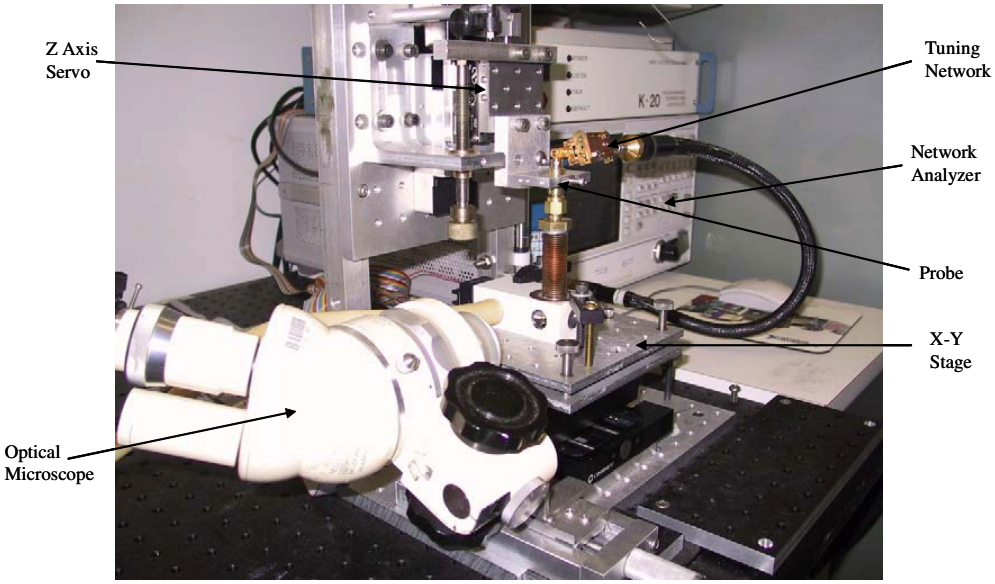

Figure 1. Evanescent microwave microscopy system.

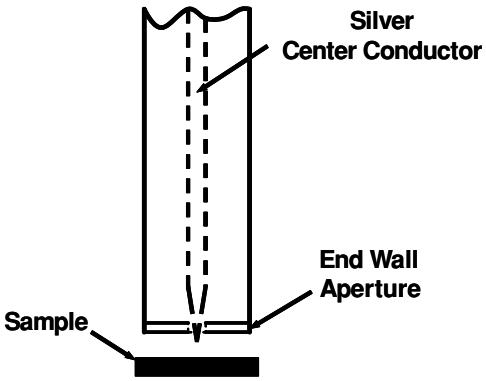

Figure 2. Probe schematic.

inside the outer shield with high-grade paraffin. A copper end-wall aperture was placed at the sharpened end of the coax. The aperture was sized for cutoff at the resonant frequencies desired and the sharpened point of the center conductor extends beyond the end-wall aperture of the resonator. The conductive, sterling silver, center conductor along with the low-loss tangent of paraffin results in a high Q coaxial transmission line resonator. It is necessary to have Q as high as possible to achieve high sensitivity. The probing evanescent field emanates from the tip, so as the tip radius decreases, the spatial resolution increases due to localization of the interaction between the tip and sample. The standing wave in the resonator is mode converted to evanescent at the reflecting face of the end-wall aperture, where the evanescent field starts decaying exponentially, but the field intensity at the tip is of sufficient amplitude to penetrate a material such as a dielectric, provided the tip–sample distance is of sufficient length.

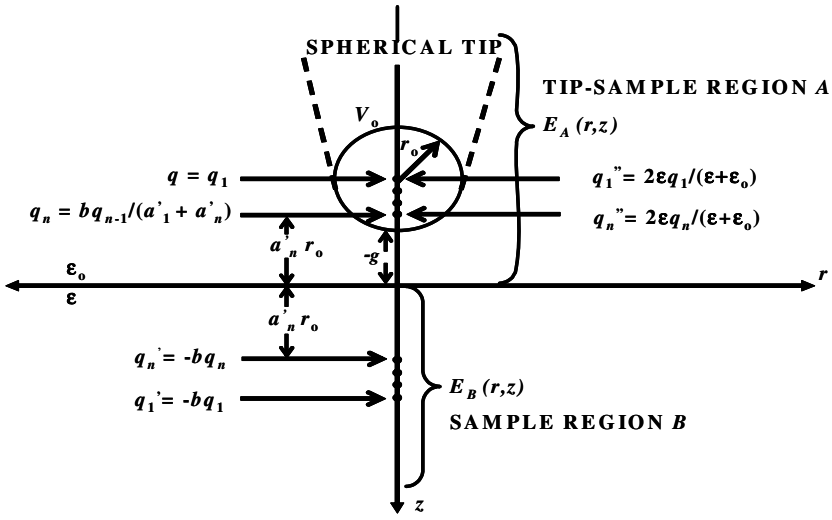

Figure 3. Image charges (q, q', q'') for a spherical tip above a sample.

The tissue-induced changes in the probe's resonant frequency, quality factor and reflection coefficient are tracked by a Hewlett–Packard 8722ES network analyzer through S_{11} port measurements, as the probe moves above the tissue sample surface. The microwave excitation frequency of the resonant probe can be varied within the bandwidth of the network analyzer and is tuned to critical coupling by external capacitors. The *X–Y* axis stage is driven with Coherent® optical encoded dc linear actuators. The probe is frame mounted to a *Z*-axis linear actuator assembly and the height at which the probe is above the sample can be precisely set. The *X–Y* stage actuators, network analyzer, data acquisition and collection are controlled by the computer. The program that interfaces to the *X–Y* stage actuators, serial port communications, 8722ES GPIB interface and data acquisition is written in National Instruments Labview® software. The complete evanescent microwave scanning system is mounted on a vibration-dampening table.

2.2. *Quantitative microwave microscopy*

The expression for the resonant frequency shift due to the presence of a material is

$$\frac{\Delta f}{f} = -\frac{\int_V (\Delta\varepsilon)(\bar{E}\cdot\bar{E}_0) + (\Delta\mu)(\bar{H}\cdot\bar{H}_0)\,\mathrm{d}V}{\int_V \left(\varepsilon_0\bar{E}_0^2 + \mu_0\bar{H}_0^2\right)\mathrm{d}V} = \frac{f - f_0}{f}, \tag{1}$$

where $\bar{E}$, $\bar{H}$ are the perturbed electric and magnetic fields, $\bar{E}_0$, $\bar{H}_0$ are the unperturbed fields, V is the volume of a region outside the resonator tip, f is the resonant frequency and f_0 is the unperturbed reference frequency.

The perturbed electric fields $\bar{E}_A$ and $\bar{E}_B$ within the tip–sample region A and the sample volume region B (figure 3.), respectively, can be derived using an iterative method described in Kleismit *et al* (2005a). Furthermore, according to Kleismit *et al* (2005a), the over all resonance frequency shift due to the perturbed electric fields $\bar{E}_A$ and $\bar{E}_B$ is given by

$$\left(\frac{\Delta f}{f_0}\right)_{A+B} = -C\sum_{n=1}^{\infty} t_n \left\{1 - \frac{1}{2}(1-b)\frac{1}{a'_1 + a'_n}\right\}, \tag{2}$$

where r_0 is the tip radius, g is a distance from the tip to the surface of the sample and $a_1' r_0 = r_0 + g$, $a_n' = a_1' - \frac{1}{a_1' + a_{n-1}'}$.

The constant C is a geometry factor of the resonator assembly and determined by the measurement methodology of Kleismit *et al* (2005a) utilizing a single crystal dielectric sample of known complex permittivity. By taking into account the real part of equation (2), we obtain the following expression to find the complex permittivity and resonant frequency change, which is used to compare with our experimental data when the tip touches the sample ($g = 0$):

$$f_r = f_0/1 + (C/4)\left(\frac{3}{2} + \sum_{n=1}^{\infty}\left[\frac{2n+5}{(n+1)(n+2)}\right]R^n \cos n\phi\right) \tag{3}$$

The change in quality factor Q is derived similarly

$$q_r = q_0/1 - (q_0)\left(\frac{C}{2}\right)\left(\sum_{n=1}^{\infty}\left[\frac{2n+5}{(n+1)(n+2)}\right]R^n \sin n\phi\right), \tag{4}$$

where

$$R = ((\varepsilon'^2 + \varepsilon''^2 - 1)^2 + 4\varepsilon''^2)^{1/2}/((\varepsilon' + 1)^2 + \varepsilon''^2)$$
$$\phi = \tan^{-1}((2\varepsilon'\varepsilon'')/(\varepsilon'^2 + \varepsilon''^2 - 1)),$$
$$\varepsilon = \varepsilon_0(\varepsilon' + \mathrm{i}\varepsilon'').$$

Equations (3) and (4) can be used to calculate the total shift in frequency and in Q to determine the real and imaginary components respectively of the local complex dielectric constant sensed by the probe tip. The total shift comprises a resonant frequency f_0 and Q_0 when the probe is not influenced by a material (unperturbed) in its near field and is due to its own self-resonance. The material is then brought into the near field of the probe and touches the tip (perturbed), resulting in a total shift in frequency to f and Q which is linearly fit between f_0, f and Q_0, Q to determine the localized complex permittivity parameters. The tissue samples are soft enough to allow the tip to touch the surface without damaging the probe, making the device unique for characterizing biological samples.

2.3. Tissue complex permittivity measurements

The porcine skin tissue samples were acquired from a local slaughter facility and the time duration from death to tissue sample characterization was less than 2 h, and tissue samples were refrigerated at approximately 40 °F during transport. The porcine tissue samples are 18 to 20 month old males of American Yorkshire type and shoulder location. A total of six measurements were made in a linear fashion with 100 μm separation between discrete measurement locations at each frequency with the tissue sample surface dry at a temperature of 289 K. A single subject was used in the study of this section.

2.4. Evanescent field depth and subsurface structure detection

A series of three line scan measurements were performed with the evanescent probe across the surface of an excised section of porcine tissue from a second separate subject, resulting in three single-line maps of the change in resonator quality factor profile of the non-uniformities, depth-wise in the tissue sample. The scan parameters for the tissue sample are resonant frequency $f_0 = 1.1373$ GHz with an average probe tip standoff distance of 5 μm above the tissue surface and 10 μm step intervals recording a resonant quality factor profile over a scan length of 2000 μm. The Q of the resonator is proportional to the changes in conductivity.

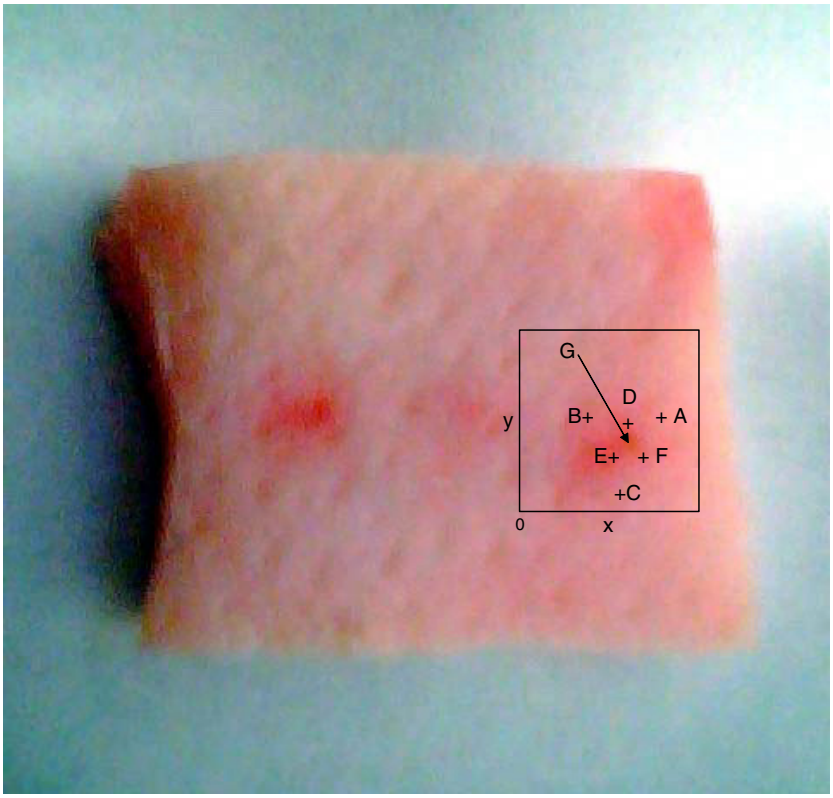

Figure 4. Scan area of the porcine skin puncture lesion.

Compared to the effect of conductivity on Q, changes in Q with variance of the tip to tissue standoff height g will be relatively small due to geometric considerations. Namely, the decay length of the evanescent field in air is 350 μm, and the decay length with the skin sample present is at least 200 μm. Therefore, a change in standoff height of 5 or 10 μm between different skin locations does not change the source of the signal arising from the large volume of skin to depths of $\sim$200 μm by more than a few percent. The resonant f_0 was chosen because it is the $\lambda/4$ fundamental frequency of the probe. Following the scans, the porcine skin was fixed in 10% formalin in phosphate-buffered saline, dehydrated in ethanol and embedded in paraffin. Sections approximately 10 μm in thickness and 2000 μm in length were mounted on glass slides and stained in hematoxylin and eosin and photographed for comparison against the line scan change in Q signature.

2.5. Scan of tissue puncture lesion and measurement

A skin surface puncture lesion from a third discrete subject shown in figure 4 was characterized in a two-step procedure. Initially the lesion was scanned with the resonant probe, producing a relative change in frequency, Q, and reflection coefficient images over the scan area. The image scan area is 3 mm $\times$ 3 mm with a probe standoff distance height of 10 μm above the tissue surface, an image resolution of 100 μm measurement steps, at a resonant frequency of 1.1373 GHz. Subsequently, complex dielectric measurements were performed using the

Figure 5. Skin surface burns (1) 600 °F 1 s, (2) 600 °F 2 s, (3) 600 °F 3 s, (4) 600 °F 4 s and (5) 600 °F 5 s.

methodology of section 2.2 and equations (3) and (4) at points of interest in the relative change in Q image. Three dielectric measurements were taken approximately 500 μm from the center of the lesion about 120° apart and indicated at points (A, B, C). The second set of three measurements were taken approximately 150 μm from the center of the lesion at roughly the same angular spacing at points (D, E, F), and the final measurement point is centered in the puncture lesion at point (G). It was noted that prior to characterization, the puncture lesion appeared to be an older wound. The puncture site had dark coagulated blood and the immediate adjacent tissue was raised and pink in color.

2.6. Complex permittivity measurements of heat damaged tissue

Figure 5 shows five separate burn areas on the surface of an excised section of porcine tissue from a fourth and final subject, where the burn areas are of increasing severity labeled 1–5. The subsurface tissue damage should vary according to the depth of involvement, resulting from acute thermal contact. The five burn marks were induced by direct contact of a tip from a standard soldering instrument. A 600 °F iron was held under constant pressure on the tissue surface from 1 to 5 s in duration. A series of complex dielectric measurements were made by moving the probe at several locations within each burn location area at a frequency of 1.1373 GHz.

3. Results and discussion

Biological tissues are inhomogeneous and exhibit considerable variability in structural composition and, therefore, dielectric properties. The ranges of complex dielectric measurements at each frequency along with the population mean (solid curve) are indicated in figures 6 and 7 for the dielectric constant and dielectric loss, respectively. The mean value of the data spread at each frequency is indicated by the solid blue curve, and the actual data are denoted by solid red points. The statistical data are based on six random readings at each frequency and given in tables 1 and 2. Due to the lengthy experimental procedure of acquiring

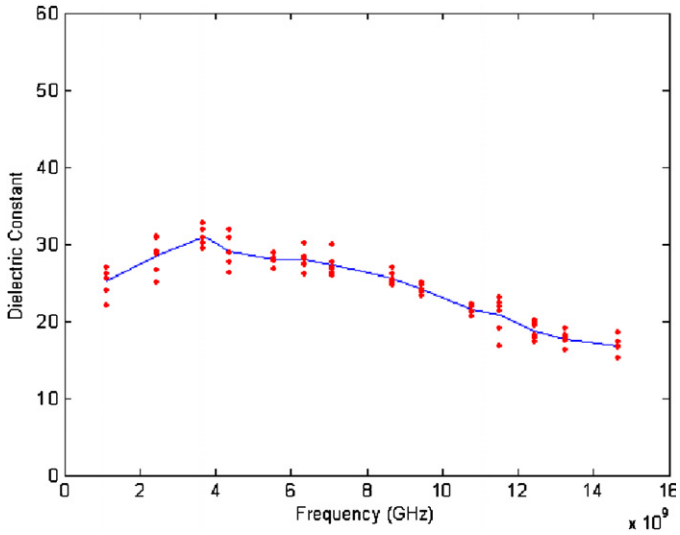

Figure 6. Dielectric constant of porcine skin tissue from 1 GHz to 15 GHz.

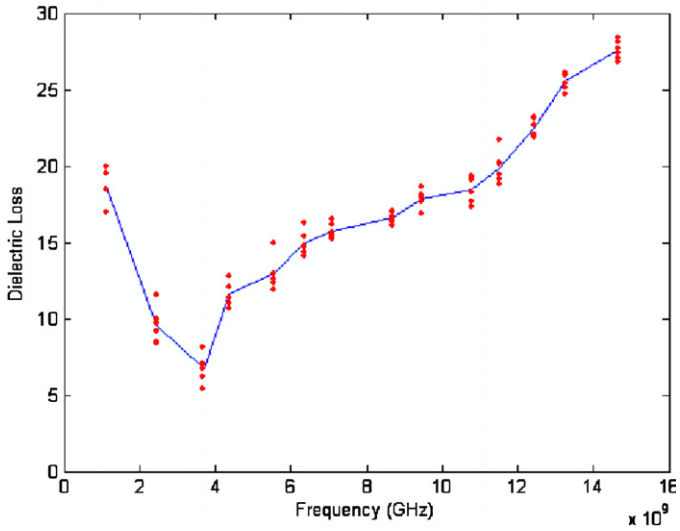

Figure 7. Dielectric loss of porcine skin tissue from 1 GHz to 15 GHz.

complex permittivity values at 15 discrete frequencies, only six data points were acquired to stay within the 2 h sample maximum, so the data would not be biased from dehydration and give a reasonable estimate of reproducibility. The dielectric constant measurement results of our investigation ranged in values from 16.5 to 38.8. The dielectric loss values ranged from 5.4 to 28.5. The range of dielectric constant values for our data is 29–33 at 3 GHz compared to 19–22 for the data represented in Olawale *et al* (2005) for 4 to 5 month old porcine specimens. The subjects used in our study were around 18 to 20 months old and, in general, we would expect the subject to be less hydrated resulting in a lower dielectric constant and loss due to

Table 1. Dielectric constant mean and standard deviation versus frequency.

Frequency (GHz)	Mean	SD
1.116	25.25	1.943
2.451	28.483	2.368
3.699	30.916	1.205
4.363	29.08	2.239
5.544	28.066	0.742
6.364	27.9	1.331
7.088	27.216	1.499
8.665	25.583	0.837
9.473	24.116	0.649
10.776	21.533	0.634
11.537	20.75	2.361
12.445	18.716	1.1354
13.246	17.7	0.883
14.865	16.783	1.11

Table 2. Dielectric loss mean and standard deviation versus frequency.

Frequency (GHz)	Mean	SD
1.116	18.667	1.402
2.451	9.549	1.146
3.699	6.75	0.909
4.363	11.6	0.851
5.544	12.933	1.081
6.364	14.933	0.806
7.088	15.733	0.516
8.665	16.633	0.377
9.473	17.867	0.56
10.776	18.483	0.849
11.537	19.9	1.031
12.445	22.483	0.594
13.246	25.533	0.56
14.865	27.583	0.604

surface lipid chemical composition changes in the skin from birth to adolescence (Ramasastry *et al* 1970). However, numerous factors, such as sample handling, animal strain, feed routine, probe sensing depth and tissue temperature, were not identical between the previous study (Olawale *et al* 2005) and the existing study and these factors may have countered the expected trend. To compare measurement reproducibility between our study and a previous study, we calculated the standard error of the mean for the measurements in tables 1 and 2 and obtained ranges of 0.025–0.966% for the dielectric constant, and 0.154–0.467% for dielectric loss. This level of variability is considerably smaller than the values of 5–10% for dielectric constant and 0.2–3% for dielectric loss (Olawale *et al* 2005). This indicates that the evanescent probe design and technique described here might be more reproducible.

The dielectric constant data measured in this study show an increase from 1 GHz to 3 GHz. and then decreases above 3 GHz. The expected trend was for the dielectric constant to decrease with increasing frequency over the entire frequency range due to γ dispersion resulting from the polarization of water molecules (Stuchly and Stuchly 1990). One possible

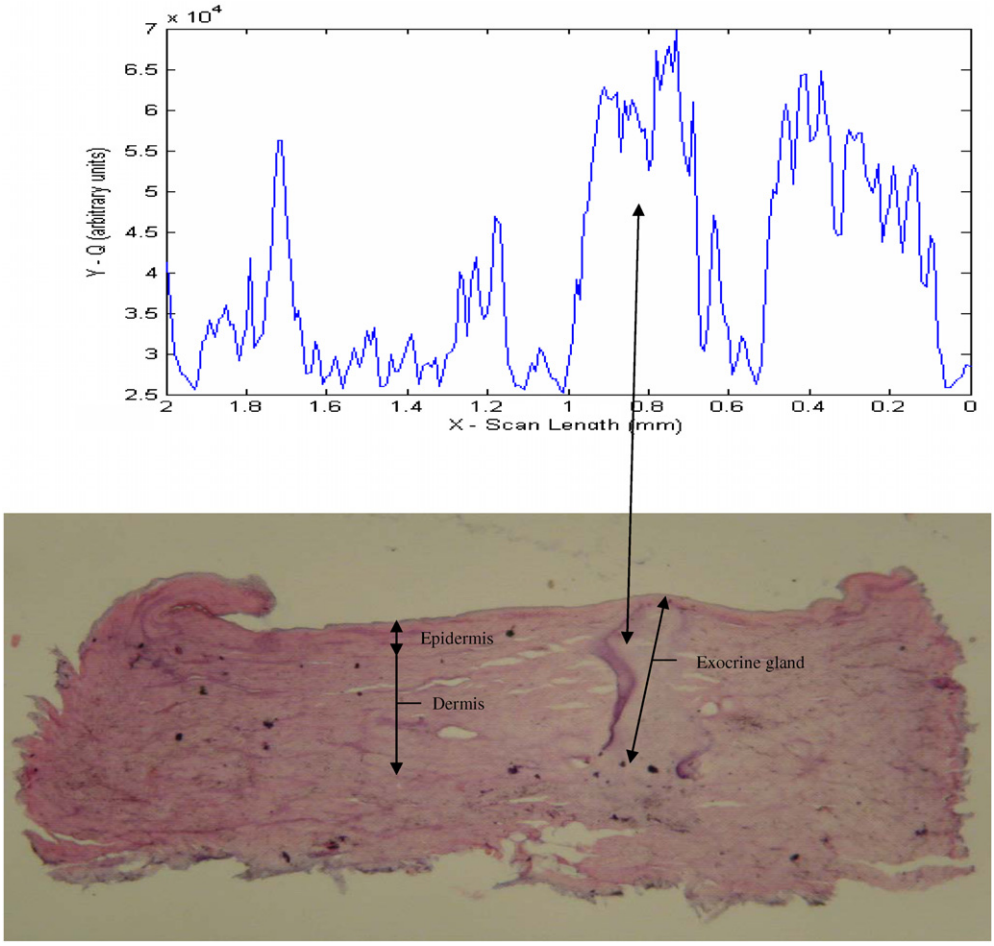

Figure 8. ΔQ line scan of tissue showing correspondence of signal peaks with capillary beds and exocrine gland.

explanation for the increase between 1 GHz and 3 GHz is that this was an artifact caused by limited tissue thickness leading to secondary field reflections. It should be noted that in a previous study (Olawale *et al* 2005), the trend in the dielectric constant between 1 GHz and 3 GHz is also not smoothly downward. At present, we feel that it is unlikely that the dielectric constant increases with frequency over this frequency range due to physical implausibility, but further studies should be performed to rule out the possibility.

Figures 8 and 9 illustrate the ΔQ line scan signal from the probe and corresponding subsurface tissue histological structure. The prepared tissue slides and line scan measurements show a relation of ΔQ (conductivity) signal strengths and corresponding biological structures such as ducts of exocrine sweat glands and vein lumen ducts. The tissue slide sample edges were curled during processing and the tissue appears to be slightly stretched, but the tissue structure-signal match up can be seen fairly well. The longest skin structure seen by the probe is the exocrine duct in figure 8 between 0.6 mm and 1.0 mm on the X-axis and extends from the surface to approximately 0.375 mm into the dermis. There is a large signal peak between 0.5 mm and 0.1 mm that could be due to a gland or vein that is out of the plane of

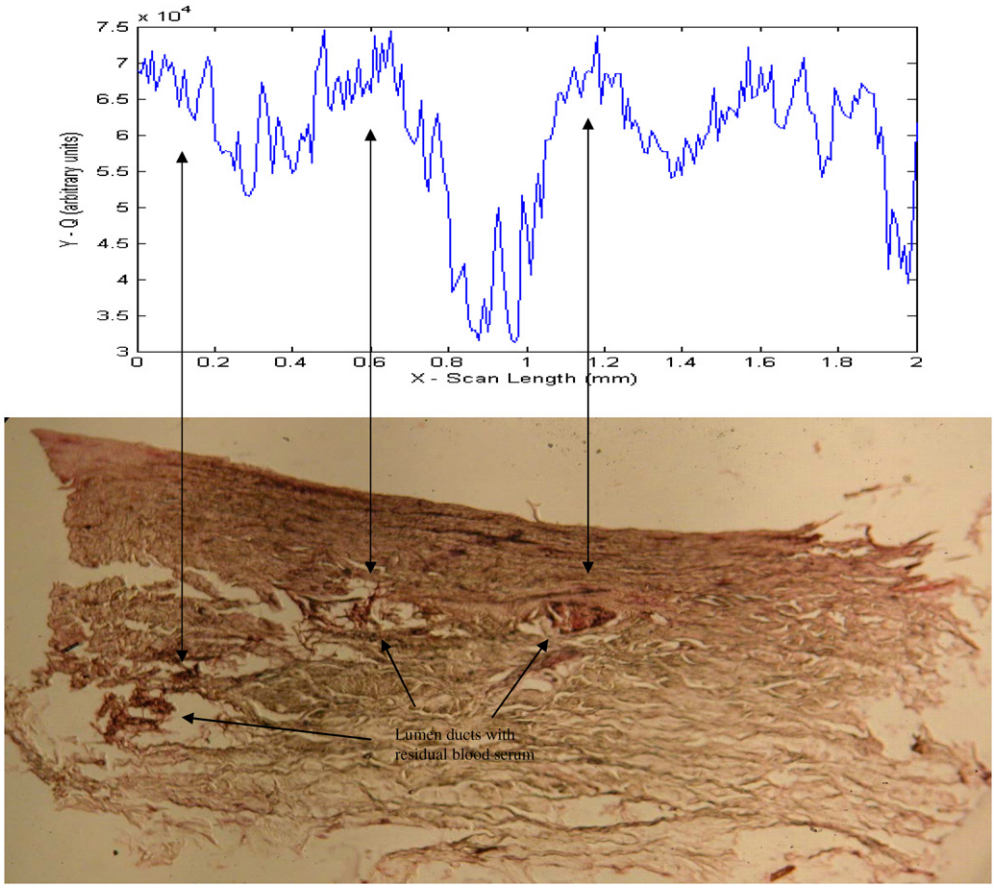

Figure 9. ΔQ line scan of tissue showing correspondence of signal peaks with the lumen of a vein moving in and out of the plane of section.

the slide since the histology slice is only 10 μm, whereas the spatial region being detected by the probe certainly includes an area wider than 10 μm due to the spreading of the field emanating off the tip (Tabib-Azar *et al* 1999b). In figure 9, there are three vein ducts, two of which are distinct, traversing the dermis tissue in the plane of the slide and are shown at 0.0–0.25 mm, 0.5–0.8 mm and 1.0–1.3 mm on the X-axis. There is also a signal peak between 1.4 mm and 1.9 mm that does not correspond to any subsurface feature in the histology slide, which again may be due to a structure outside of the plane of the slide. The depths of the vein lumen are approximately from 0.25 mm to 0.3 mm. The majority of the smaller signal peaks may correspond to capillary beds near the surface, which reveal residual blood serum from the staining process and are considered more conductive than dielectric and/or spatial heterogeneity. The capillary beds are located under the epidermis layer and have an average depth of 35 μm. However, the source of these small fluctuations with position is not entirely clear and may also include contributions from variations in probe-to-skin standoff height or other types of biological variability with position. The probe tip radius is 10 μm and the spatial resolution of the probe is governed by this physical dimension, but the aperture diameter along with the tissue properties dictates the evanescent field decay length. The corresponding ΔQ

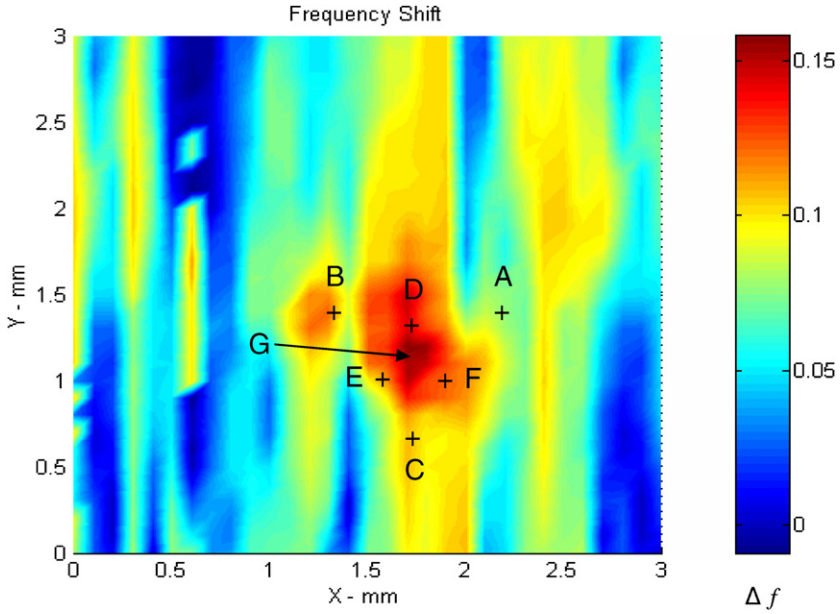

Figure 10. Change in the frequency image of the tissue puncture lesion.

signal widths will be slightly larger than the lumen ducts and gland structures the evanescent field detects at tissue depths within the decay length of the field, due to the three-dimensional penumbral effect of the field emanating off the probe tip and widening depth-wise. This sensor appears that it could be used for superficial wound and burn assessment, but as far as the applicability to deep lacerations, the device is presently limited from deep field penetration depth.

The surface puncture lesion of figure 4 was scanned, producing a change in the resonance frequency, Q, and reflection coefficient images illustrated in figures 10–12, respectively. The change in the frequency image contains surface topography and dielectric properties, while the change in the Q image shows the variations in conductivity, which is the inverse of the change in the reflection coefficient image and indicates the resistive properties of the tissue sample. The total shift in resonant frequency and Q measurements was model fit, resulting in dielectric property values on and around the puncture lesion for seven separate locations. The real and imaginary parts of the complex dielectric measurement are given in table 3. The outermost points (A–C) are comparable to normal tissue values. The immediate surrounding data (D–F) indicate a higher conductivity and lower dielectric constant, than measured at this frequency in normal tissues (figures 6 and 7, tables 1 and 2). The measurement of the puncture lesion indicate a low conductivity and a high dielectric constant at point G, which is centered on the puncture wound and corresponds to dry coagulated blood cells. The age of the puncture wound and the possibility of dilated and leaking capillary beds and/or infection could explain the higher conductivity readings in the immediate surrounding tissue.

The tissue surface burn data shown in table 4 for section 1 shows a higher dielectric constant and slightly lower related loss in comparison to the normal tissue values. This result could be an effect of reducing moisture in the outermost epidermal layer. Section 2 data show an increase in conductivity and a decrease in dielectric constant from the data for section 1. A possible explanation is a further thermal disruption of the skin, releasing water, ions and

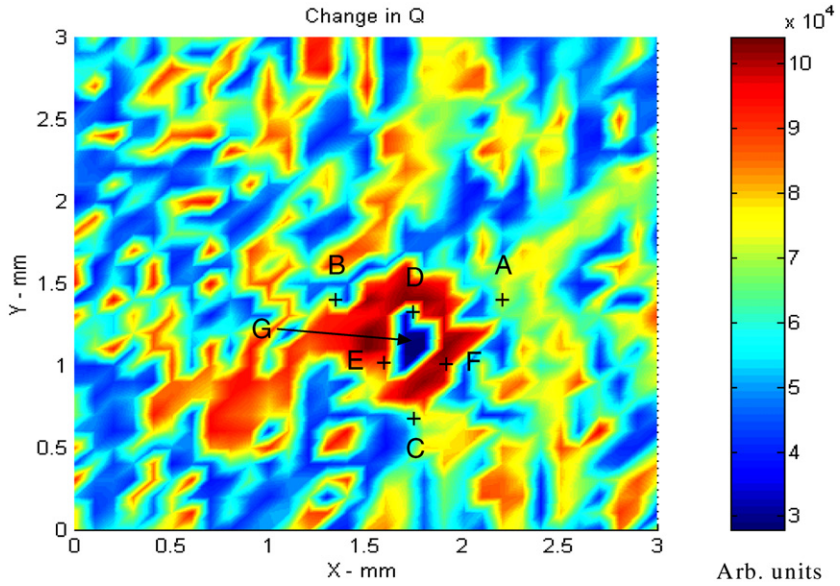

Figure 11. Change in the Q image of the tissue puncture lesion.

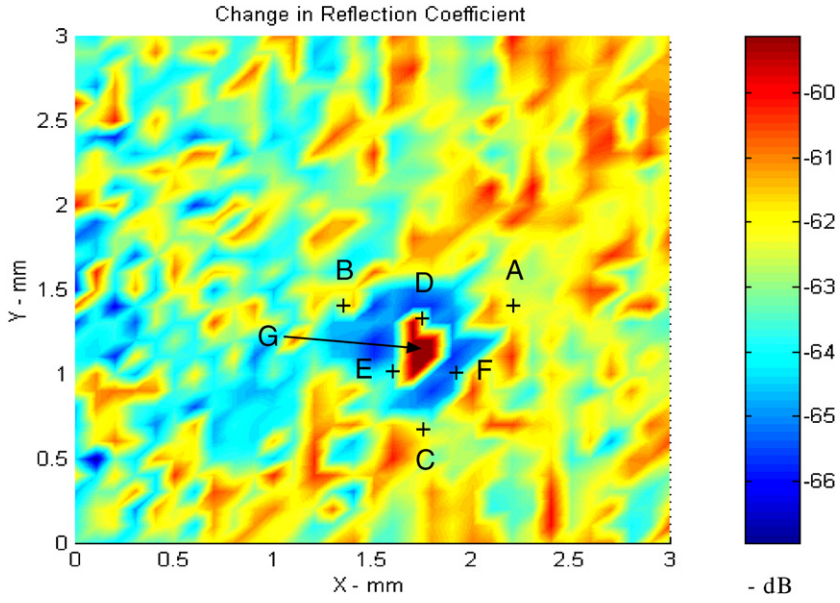

Figure 12. Change in the S_{11} image of the tissue puncture lesion.

plasma proteins from the interstitial fluid due to tissue denaturing and micro vascular damage (Devgan *et al* 2005). The data of section 3 show a significant decrease in conductivity, which may be due to additional fluid evaporation and thickness damage. The burn data of

Table 3. Tissue puncture lesion measurements and location.

Sample point	Dielectric constant	Dielectric loss	Lesion center dist. (mm)
A	26.1	20	500
B	19	21.7	500
C	27	18.7	500
D	17.9	23.7	150
E	17.5	24.1	150
F	18.2	23.4	150
G	38	2.1	0

Table 4. Tissue burn lesion section measurement mean.

Section	Dielectric constant (mean)	Dielectric loss (mean)
1	45.22	16.6
2	32.98	19.98
3	37.8	3.25
4	21.38	2.82
5	8.68	0.304

sections 4 and 5 indicate a continued decrease in dielectric constant and loss from interstitial fluid evaporation and thermal degradation of the tissue.

4. Conclusion

This experimental exercise produced dielectric constant and loss measurements that were carried out *in vitro* on freshly excised tissue. The technique used in this study produced dielectric and conductivity values and trends for porcine skin tissue consistent with those seen by the open-ended coaxial technique. The results indicate that this technique could be used for superficial wound assessment, but as far as the applicability to deep wounds the device is presently limited by penetration depth. The burn data indicate appreciable dielectric property differences with thermal damage levels and show promise that the evanescent technique could be used for burn evaluation. Although the research was conducted *in vitro* and live tissue exhibits full physiological and anatomical functional activity when burned, an *in vivo* study may still produce significant enough thermal level data differences to make the technique useful. The probe indicates a capability to detect capillary beds and veins within the tissue from conductivity signatures; therefore it is conceivable that this may be extended in utilizing the sensor in monitoring skin tumor angiogenesis and performance of endogenous inhibitors.

References

Anlage S, Steinhauer D, Feenstra B, Vlahacos C and Wellstood F 2001 Near-field microwave microscopy of materials properties *Microwave Superconductivity* ed H Weinstock and M Nisenoff (Amsterdam: Kluwer) pp 239–69

Devgan L, Bhatt S, Aylward S and Spence R 2005 Modalities for the assessment of burn wound depth *J. Burns Wounds* **5** 7–15

Gabriel C, Gabriel S and Corthout E 1996a The dielectric properties of biological tissues: I. Literature survey *Phys. Med. Biol.* **41** 2231–49

Gabriel S, Lau R and Gabriel C 1996b The dielectric properties of biological tissues: II. Measurements in the frequency range 10 Hz to 20 GHz *Phys. Med. Biol.* **41** 2251–69

Gao C and Xiang X 1998 Quantitative microwave near-field microscopy of dielectric properties *Rev. Sci. Instrum.* **69** 3846–51

Gao C and Xiang X 2002 Quantitative complex electrical impedance microscopy by scanning evanescent microwave microscope *Mater. Charact.* **48** 117–25

Kleismit R, Kozlowski G, Biggers R, Maartense I, Kazimierczuk M and Mast D 2005a Characterization of local dielectric properties of superconductor $YBa_2Cu_3O_{7-\delta}$ using evanescent microwave microscopy *IEEE Trans. Appl. Supercond.* **15** 2915–18

Kleismit R, ElAshry M, Kozlowski G, Amer M, Kazimierczuk M and Biggers R 2005b Local dielectric and strain measurements in $YBa_2Cu_3O_{7-\delta}$ thin films by evanescent microscopy and Raman spectroscopy *Supercond. Sci. Technol.* **18** 1197–1203

Olawale K, Petrell R, Michelson D and Trites A 2005 The dielectric properties of the cranial skin of five young captive stellar sea lions and a similar number of young domestic pigs and sheep between 0.1 and 10 GHz *Physiol. Meas.* **26** 627–37

Ramasastry P, Downing D, Pichi P and Strauss J 1970 Chemical composition of human skin surface lipids from birth to puberty *J. Invest. Dermatol* **54** 139–44

Stuchly M and Stuchly S 1990 Electrical properties of biological substances *Biological Effects and Medical Applications of Electromagnetic Energy* ed O Gandhi (Englewood Cliffs, NJ: Prentice-Hall)

Tabib-Azar M, Akinwande D, Ponchak G and Leclair S 1999a Novel physical sensors using evanescent microwave probes *Rev. Sci. Instrum.* **70** 3381–6

Tabib-Azar M and LeClair S 1999 Novel hydrogen sensors using evanescent microwave probes *Rev. Sci. Instrum.* **70** 3707–13

Tabib-Azar M, Pathak P, Ponchak G and Leclair S 1999b Nondestructive superresolution imaging of defects and nonuniformities in metals, semiconductors, dielectrics, composites, and plants using evanescent microwaves *Rev. Sci. Instrum.* **70** 2783–92